IEEE Access
Multidisciplinary ⋮ Rapid Review ⋮ Open Access Journal

Received 7 January 2024, accepted 23 January 2024, date of publication 26 January 2024, date of current version 5 February 2024.

Digital Object Identifier 10.1109/ACCESS.2024.3358819

RESEARCH ARTICLE

All-Textile Broadband Circularly-Polarized 2 × 2 Array Antenna Based on Metasurface

TU TUAN LE, YONG-DEOK KIM, AND TAE-YEOUL YUN, (Member, IEEE)
Department of Electronic Engineering, Hanyang University, Seoul 133-791, South Korea
Corresponding author: Tae-Yeoul Yun (taeyeoul@hanyang.ac.kr)

This work was supported by the National Research Foundation of Korea 2018R1A5A7025522.

ABSTRACT This paper presents the design and analysis of an all-textile broadband circularly polarized array antenna based on metasurface (MTS), which offers a promising solution for developing a high-performance, lightweight, and comfortable antenna for various wearable applications. The array antenna configuration comprises 2 × 2 MTS elements, a ground plane, and a sequential feeding network. The MTS radiator of the antenna element is first designed and miniaturized by implementing diagonal slits. It is fed from a 50 Ω microstrip line through different-length cross-slot etched in the center of the ground plane, which has a narrow axial ratio bandwidth (ARBW). To enhance the antenna performances, the MTS array antenna is formed into a 2 × 2 arrangement. Its radiators are fed by a 90° phase difference sequential series-feeding network. The measured impedance bandwidth (IBW) of 72% on the human body is achieved, and the measured ARBW of 47.9% on a phantom head is achieved. High broadside gain and moderate radiation efficiency are observed within the ARBW. Simulated specific absorption rates (SARs) under US and European standards are below the safe level. The simulated and measured results show very good agreement.

INDEX TERMS Array antenna, circular polarization, metasurface, sequential feeding network, wearable antenna.

I. INTRODUCTION

Wearable technology has significantly advanced in recent years, resulting in a demand for wearable antennas that are conformal, comfortable, and lightweight. The wearable antenna plays a critical role in enabling wireless connectivity and communication for wearable devices. It ensures reliable transmission and reception of signals, allowing the device to interact with other devices, networks, and the internet. Efforts have been made to design wearable antennas using various materials, such as felt, polyimide, polydimethylsiloxane, and conductive fabric, for seamless integration with the wearer. However, the deformation of these flexible antennas and unpredictable human body movements can result in issues such as multipath distortion and polarization mismatch.

To address these issues, wideband antennas with circularly polarized (CP) radiation have been proposed as a more suitable solution for wearable applications. A CP antenna is more preferred because it has many advantages compared to the linear polarization (LP), including reduce multi-path interference, mitigate polarization mismatch, and maintain communication link between the wearable device and external hub. The CP excitation for wearable application is utilized by several techniques, which can be classified into radiating element and feeding network types. In terms of the former type, various antenna shapes, including the monopole antenna [1], [2], button-antenna [3], [4], and magneto-electric dipole [5], coplanar waveguide (CPW)-fed [6], [7] have been presented. Nowadays, metasurface (MTS) [8], [9], [10], [11] has been widely employed in wearable antenna design to excite CP radiation and enhance impedance bandwidth (IBW), gain, radiation efficiency, and specific absorption rate (SAR). However, the wearable CP antenna based on MTS suffers narrow axial-ratio bandwidth (ARBW). To address this issue, a sequentially rotated feeding technique [12], [13] is adopted to excite broadband CP radiation. The 90° different

The associate editor coordinating the review of this manuscript and approving it for publication was Ravi Kumar Gangwar.

sequentially rotated feeding network can enhance the ARBW because the signal is fed to adjacent elements in the array antenna with precisely controlled phase and amplitude. The relative phase different between each element is kept at 90° over the wide range of frequency with the similar amplitude and the feeding phase changes are accurate only for the desired sense of polarization, which results in producing wide ARBW. In addition, by optimizing the spacing element and rotating the antenna elements in 0°, 90°, 180°, and 270° fashion, which allows cancellation of the mutual coupling, resulting in wide bandwidth and high gain [14]. This technique is applied in wearable antenna design in [15]. An array of a 2 × 2 square patch is fed by aperture coupling through the sequentially rotated feeding slots on the ground, resulting in the broadband CP performance. However, the measured IBW of the array antenna does not fully cover the ARBW.

Characteristic mode analysis [16] (CMA) is an effective method used in the field of electromagnetics to effectively analyze the working mechanism and behavior of the MTS. The characteristic modes are independent of any kind of excitation, e.g., feeding structures; they only depend on the size and shape of the conducting object for the MTS. The understanding on the physical behavior of the radiator have been used to enhance the antenna performances. Recently, CMA is also applied on the wearable antenna design in [17], [18]. In [17], the current and strength of the current in a 3 × 3 nonuniform MTS array are analyzed varying with the change of the rotation angle of each unit cell with the assistant of CMA. In [18], CMA is used to study the parasitic patch, the driven patch, and the parasitic strip of the transparent antenna. Both antennas are designed covering 5.85-GHz WBAN. However, these antennas only radiate LP wave.

In this paper, an approach is proposed to excite broadband CP radiation, which utilizes MTS and 90° phase difference sequentially rotated feeding network. The single MTS antenna is first designed by CMA, which excites two broadband degenerate modes but not fully cover the ARBW for a targeting bandwidth including 5.15–5.85 GHz and a part of ultra-wideband (UWB) for wireless body-area network (WBAN) applications. Then, the 2 × 2 metasurface array is placed on the top substrate as the primary radiating element. It is fed from aperture coupling through the sequentially rotated feeding slots on the ground plane. The feeding network is placed on the bottom substrate. The proposed antenna design is fabricated using low-cost textile materials, making it lightweight and comfortable to wear. The fabricated antenna is measured in free space, as well as on the human body and phantom head. This research presents the method to achieve a broad bandwidth, high performance, and low SAR wearable antenna, making it suitable for various wearable applications.

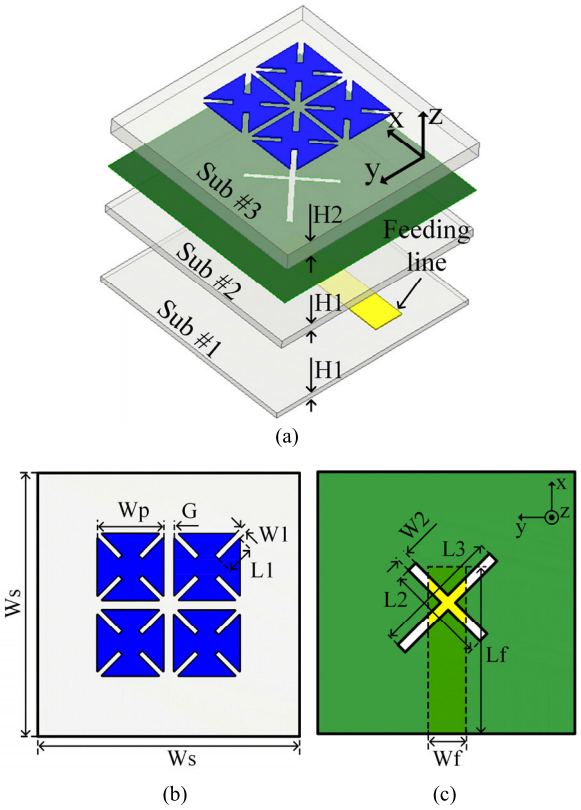

FIGURE 1. The geometry configuration of the single MTS antenna: (a) perspective view, (b) top view of MTS layer, and (c) top view of orthogonal-slot ground plane layer.

II. SINGLE MTS ANTENNA DESIGN AND MECHANISM

A. SINGLE MTS ANTENNA

The geometry of the single MTS is shown in Fig. 1. The single MTS antenna consists of an MTS layer, an orthogonal-slot ground plane, a 50 Ω microstrip line, and a multi-layer felt substrate. All conductors are made of Shieldit™super conductive textile with a conductivity of 118,000 S/m. A thin Sub#1 works as an isolator to reduce the proximity effect from the human body. The MTS comprises 2 × 2 diagonal-slit square-patch unit-cells placed on the top side of Sub#3, as shown in Fig. 1 (b). The slits introduce additional capacitance to miniaturize the MTS [19]. A different-length cross-slot is etched in the center of the ground plane, as shown in Fig. 1 (c). It couples electromagnetic energy and introduces perturbation to the MTS antenna. A 50 Ω microstrip line and a ground plane are attached on the bottom and the top side of Sub#2, respectively. The conductors are designed on the felt substrate. The felt substrate has a dielectric constant of 1.4, a loss tangent of 0.044. The optimized values of the proposed antenna are listed as follows:

H1 = 1.5, H2 = 3, Ws = 40, Wp = 10, G = 1, W1 = 1, L1 = 4.5, L2 = 15, L3 = 20, W2 = 1, and Lf = 24 (unit: mm).

B. CHARACTERISTIC MODE ANALYSIS OF THE MTS

CMA is a unique method that present the electromagnetic properties of the structures without determining the source of excitation. The modal significance (MS_n) is the

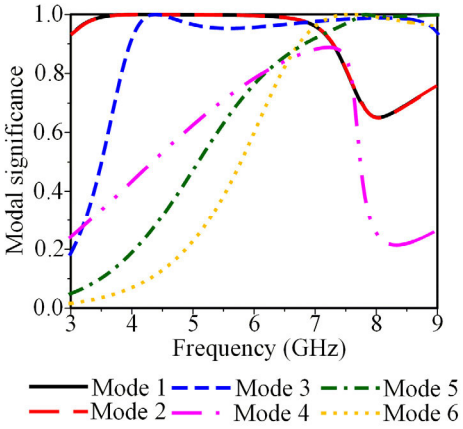

(a)

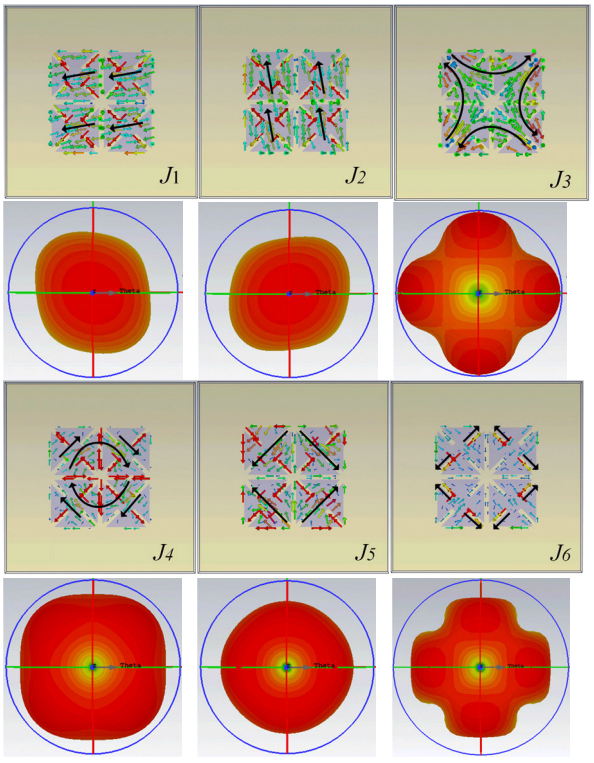

(b)

FIGURE 2. CMA of the single MTS antenna: (a) modal significance and (b) current distributions and 3D radiation pattern in different modes.

important parameter, as a function of eigenvalue. The modal significance ($MS_n = 1/|1 + j\lambda_n|$), where λ_n is the eigenvalue, is an important parameter. The operating bandwidth of a nth mode is defined as $MS_n > 0.7$. The closer MS_n is to 1, the greater is the efficiency of the antenna radiation.

Fig. 2 presents MS_n, the current distribution, and the 3D radiation pattern in the first six modes, J_1–J_6, from 3 to 9 GHz of the proposed MTS. As shown in Fig. 2 (a), the modal significances of J_1 and J_2 are a pair of degenerate modes, which have an identical MS value. The modal significance values are larger than 0.7 in most of the frequency band

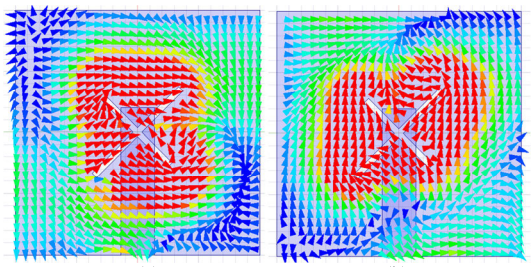

(a) (b)

FIGURE 3. Current distributions on the ground plane at (a) t = 0 and (b) t = T/4.

from 3 to 9 GHz, which indicates a broad operating bandwidth. In addition, J_1 and J_2 have a directional radiation pattern, as shown in Fig. 2 (b). The modal current of J_1 is in-phase and radiates in x-polarization. Similar to J_1, the modal current of J_2 is in-phase but radiates in y-polarization. It is clearly observed that J_1 and J_2 have similar radiation patterns but orthogonal polarization states because they have orthogonal current distributions. According to [20] and [21], CP radiation can be implemented by exciting J_1 and J_2 with a 90° phase difference.

Meanwhile, the modes of J_3, J_4, J_5, and J_6 have null radiations in the broadside direction because the current distributions are out-of-phase at the center. Therefore, J_3, J_4, J_5, and J_6 have omni-directional radiation patterns, as shown in Fig. 2 (b).

C. FEEDING METHOD OF THE SINGLE MTS ANTENNA

As discussed in the previous section, J_1 and J_2 are a pair of degenerate modes. The CP operation can be realized by exciting J_1 and J_2 with a 90° phase difference. The surface currents of J_1 and J_2 are evenly distributed in x- and y-directions, respectively. Therefore, J_1 and J_2 can be excited by placing the excitation source immediately below each square-patch unit-cell. Meanwhile, the modes J_3–J_6 are out-of-phase at the center and concentrate around the edge of the MTS, which makes it difficult to excite them. The degenerate mode can be excited by introducing perturbation using diagonal-slot feeding [22], [23]. Therefore, the feeding method that includes a 50-Ω microstrip line and a non-uniform cross-slot feed is employed, as shown in Fig. 1(c). The current distributions on the ground plane at two different time instances of t = 0 and T/4, where T is the period of time at 5.8 GHz, are shown in Fig. 3. The surface currents at t = 0 are strongly distributed in the x - direction, which excites the J_1 mode. Meanwhile, the surface currents at t = T/4 are distributed in the y-direction, which excites the J_2 mode. The simulated |S11| and |AR| of the single MTS antenna are 43.62% (4.75–7.40 GHz) and 5.42% (5.74–6.06 GHz), respectively, as shown in Fig. 4. The ARBW of the single MTS antenna is somewhat narrow. To improve the antenna performance, including the ARBW, an array MTS antenna for wearable applications is proposed in Section III.

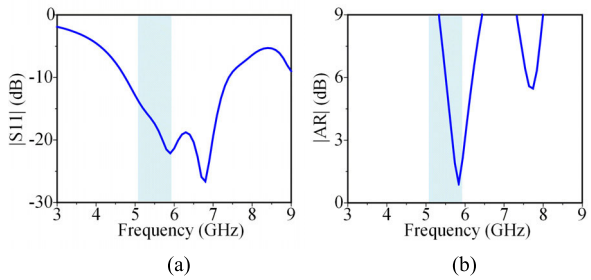

FIGURE 4. Simulated results of the single MTS antenna: (a) S11 and (b) AR.

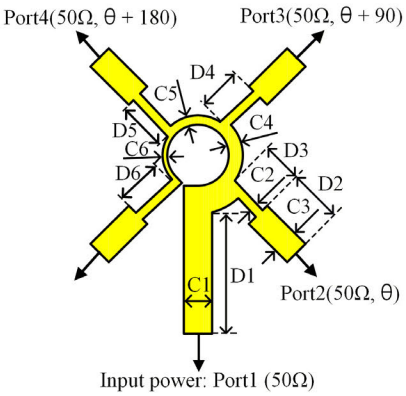

FIGURE 5. The geometry of the 1-to-4 sequential feeding network.

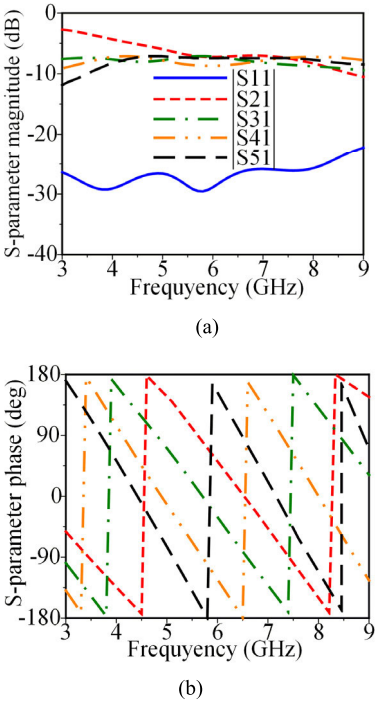

FIGURE 6. Simulated S-parameters of the feeding network in: (a) magnitude and (b) phase.

III. MTS ARRAY ANTENNA AND DEFORMATION STUDY

A. ARRAY ANTENNA USING SEQUENTIAL FEEDING NETWORK

Fig. 5 shows the geometry of the proposed serial 1-to-4 sequential feeding network using a compact open ring [24]. The output ports of the feeding network are formed in counter-clockwise direction to generate right-hand CP (RHCP) waves. The feeding network is designed with serially connected microstrip lines with different impedance characteristics. The width of the series-microstrip line and the quarter wavelength transformer are optimized for achieving 90° phase difference and equal amplitude at the output ports. The simulated S-parameter amplitude and phase of the feeding network are shown in Fig. 6. The return loss of the feeding network is below −20 dB. The signal from the input port, Port1, is equally delivered to four output ports, Ports 2–5. Similar transmission coefficients of |S21|, |S31|, |S41|, and |S51 are observed from 5 to 8 GHz with the value ranging from −5.5 to 8.5 dB, as shown in Fig. 6 (a), with a phase difference of 90°, as shown in Fig. 6 (b). The optimized values of the feeding network are listed as below:

C1 = 6, C2 = 2, C3 = 3, C4 = 2, C5 = 1, D1 = 25.8, D2 = 11.5, D3 = 8.6, D4 = 9.6, D5 = 10.6, D6 = 11.4 (unit: mm).

The geometry of the 2 × 2 MTS array antenna is shown in Fig. 7. The MTS array antenna is formed by rotating the single MTS antenna with an angle of 45° around its center and then continuing rotation 90° around its z-coordinate, as shown in Fig. 7 (a). The signal from the feeding network is electromagnetically coupled with the MTS array antenna through a sequentially rotating non-uniform cross-slot in the ground plane, as shown in Fig. 7 (c). The spacing between each element is P0, which is the important parameter to determine the mutual coupling between each MTS antenna element without degrading the antenna radiation pattern. The parametric study of P0 on antenna performances including |S11|, AR, broadside gain, and radiation efficiency is shown in Fig. 8. As a result, the best antenna performance is achieved at P0 of 36 mm that is approximately equal to 0.65 λ_g, where λ_g is the guided wavelength at lowest resonant frequency of ARBW.

A comparison of the simulated reflection coefficient, AR, and broadside gain between the single and MTS array antenna is shown in Fig. 9. It is observed that the performance of the MTS array is significantly enhanced, unlike that of the single antenna. The IBW and ARBW of the MTS array are 78.4% (3.71–8.49 GHz) and 53% (4.65–8.0 GHz) compared to 43.6% (4.75–7.4 GHz) and 5.42% (5.74–6.06 GHz) of the single antenna, respectively. The maximum broadside gain within the ARBW of the array antenna is 10 dBic compared to 6.4 dBic of the single antenna.

B. DEFORMATION STUDY

In some practical situations, the antenna is mounted on curvature surfaces, which causes the deformation while operating. This section investigates the antenna performances in bending condition in the x– and y–direction with the bending

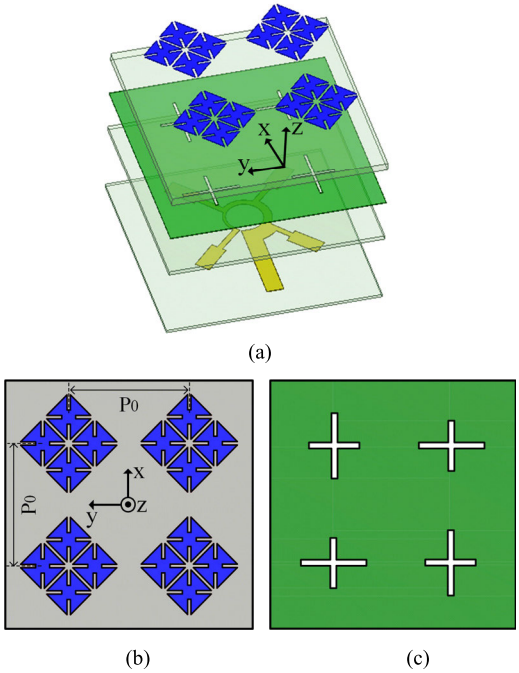

FIGURE 7. The geometry configuration of the proposed MTS array antenna: (a) perspective view, (b) top view of MTS layer, and (c) top view of ground-plane layer.

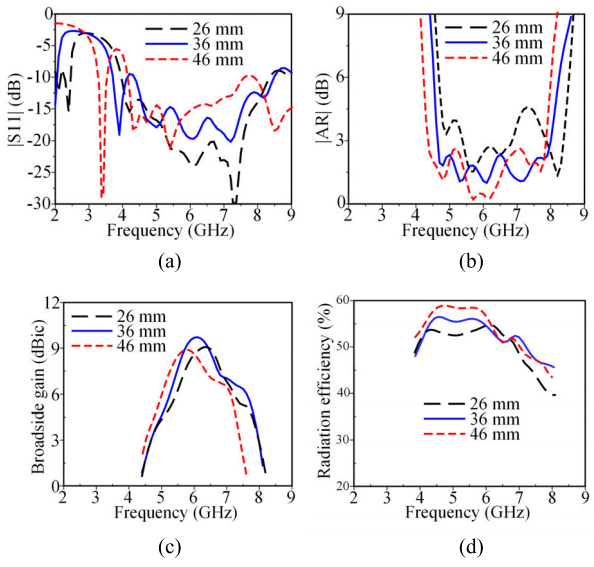

FIGURE 8. Parametric study of P0 on the antenna performance: (a) |S11|, (b) AR, (c) boadside gain, and (d) radiation efficiency.

radius of 40, 50, 60, 70, and 80 mm. The comparisons between degrees of bending for |S11| and AR are shown in Figs. 10 and 11.

It can be observed that bending in x–direction lightly affects the antenna performance because the geometry of the feeding network is nearly maintained. The 3-dB ARBW is satisfied with all the bending radius in x–direction.

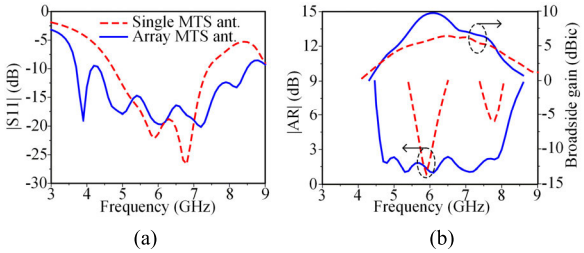

FIGURE 9. Comparison between the single and array MTS antenna: (a) |S11| and (b) AR and broadside gain.

Meanwhile, the antenna performances are strongly affected when bending in y–direction and the bending radius of less than 70 mm. Bending along y-direction asymmetrically deforms the feeding network, which does not evenly distribute the energy from input port to the output ports with 90° phase difference. When the bending radius is larger than or equal to 80 mm, the 3-dB ARBW is satisfied.

IV. ANTENNA PERFORMANCE

To demonstrate the design of the proposed MTS array antenna, the antenna is fabricated and verified by measurement in free space, human-body, and phantom-head environments.

A. FREE SPACE PERFORMANCE

The proposed antenna is fabricated by using a laser cutting technique to produce a precise prototype as shown in Fig. 12. The comparison between measured |S11| parameters in the free space and simulated result is shown in Fig. 13. The measured S11 in free space has the IBW of 97.44% (3.41–9.89 GHz), compared to simulated result of 78.4% (3.71–8.49 GHz). The comparison between simulation and measurement result in free space of ARBW, broadside gain, and radiation efficiency are shown Fig. 14. The measured ARBW is achieved of 52.6% (4.6–7.9 GHz), compared to 53% (4.65–8.0 GHz) of the simulated result. The measured radiation efficiency in free space within the ARBW ranges from 53% to 58%. Meanwhile, the measured broadside gain within the ARBW ranges from 4.9 to 9.2 dBic. The measured radiation patterns at 5.85 and 7.0 GHz the MTS array antenna in two principle *x-z* and *y-z* planes are shown in Fig. 15. It is observed that the proposed MTS array antenna radiates RHCP waves. The measured front-to-back ratios (FBR) in the broadside direction at 5.85 and 7.0 GHz are 22.5 and 17 dB, respectively.

B. ON HUMAN BODY AND PHANTOM HEAD PERFORMANCES

In this section, the antenna performances are measured on the human body and phantom-head. The proposed antenna is simulated on the four-layered tissue with a volume of 200 × 200 × 50 mm^3 as shown in Fig. 16. The tissue model includes skin, fat, muscle, and bone with thickness of 1.5, 8.5, 27.5,

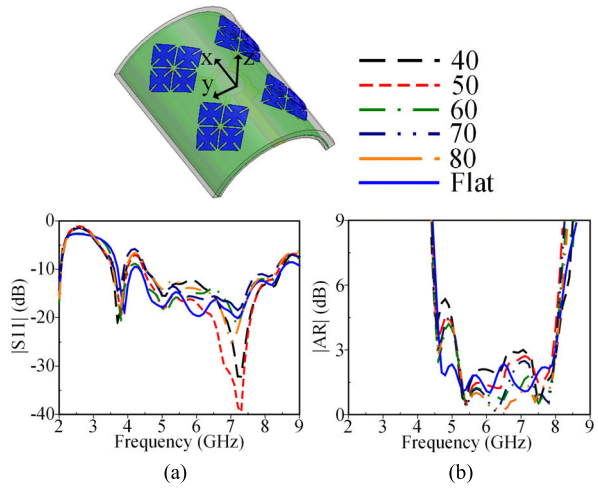

FIGURE 10. Bending effect of the proposed antenna in the *x*-direction: (a) |S11| and (b) |AR|.

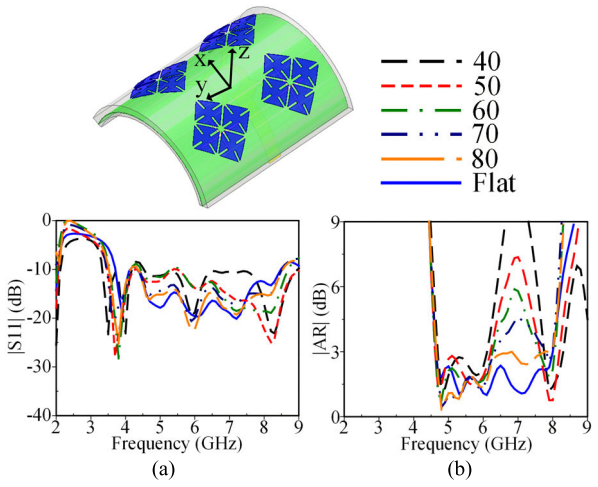

FIGURE 11. Bending effect of the proposed antenna in the *y*-direction: (a) |S11| and (b) |AR|.

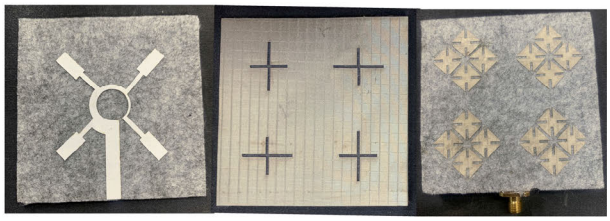

FIGURE 12. Fabricated MTS array antenna.

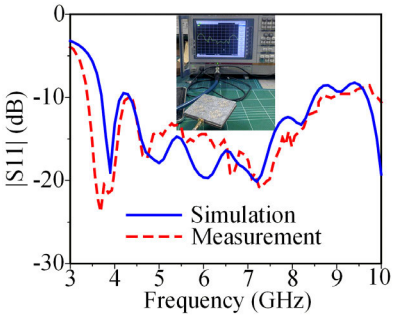

FIGURE 13. Measured S11 results in free space.

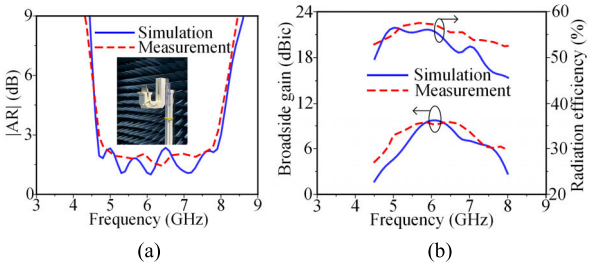

FIGURE 14. Measured results: (a) AR and (b) broadside gain and radiation efficiency in free space.

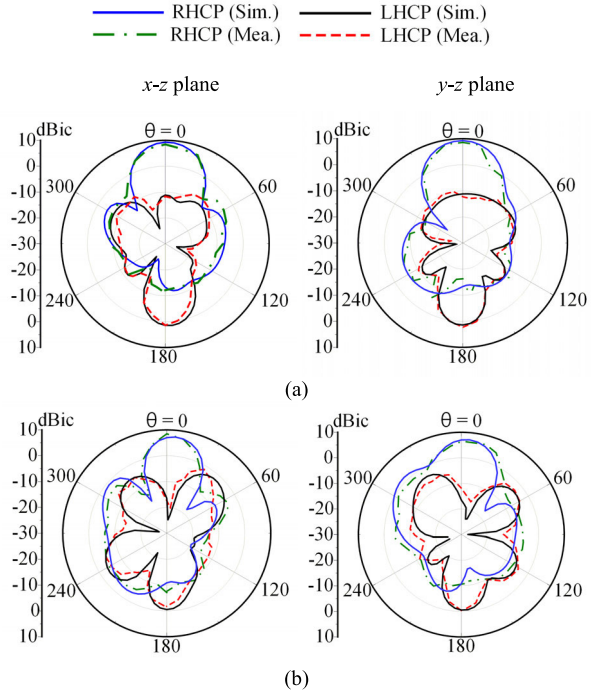

FIGURE 15. Measured radiation pattern at (a) 5.85 GHz and (b) 7.0 GHz in free space.

and 12.5 mm, respectively. The proposed array antenna is placed 5 mm above the tissue model. The permittivity and conductivity [25] of the tissue are listed in Table 1.

The measured |S11| on different body parts including chest, shoulder, and lap is shown in Fig. 17. The shape of measured |S11| on human body is somewhat identical because of the presence of isolator substrate. The measured |S11| in human chest is achieved of 72% (4.61-9.8 GHz), which is slightly less than measured result in free space. The measured AR, broadside gain, and radiation efficiency on phantom head are shown in Fig. 18. The measured ARBW is 47.9% (5–8.15 GHz), compared to 53.34% (4.77-8.24 GHz) simulated result on the tissue model. The measured broadside gain

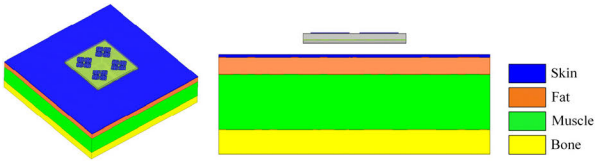

FIGURE 16. The four-layered tissue model.

TABLE 1. Human tissue.

Layer	Permittivity (ϵ_r)	Conductivity (S/m)
Skin	33.8	3.84
Fat	4.2	0.28
Muscle	50	6.48
Bone	15.8	1.77

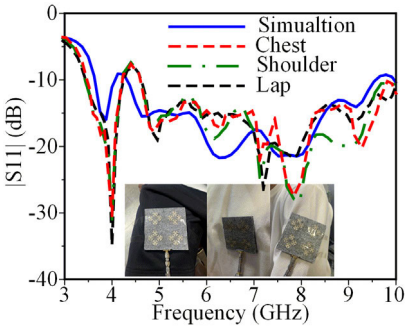

FIGURE 17. Measured S11 in human body.

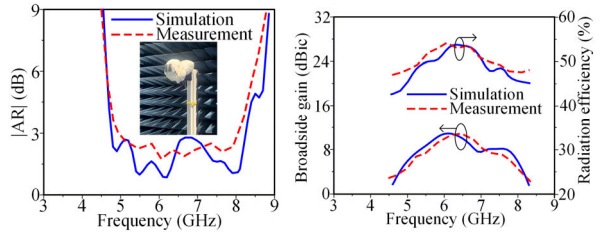

FIGURE 18. Measured results: (a) AR and (b) broadside gain and radiation efficiency in phantom head.

within the ARBW ranges from 5.1 to 11.2 dBic. Meanwhile, the measured radiation efficiency is from 50 to 56%. The measured radiation patterns on the phantom-head environments of the MTS array antenna in *x*-*z* and *y*-*z* planes are shown in Fig. 19. The measured front-to-back ratios (FBR) in the broadside direction at 5.85 and 7.0 GHz are 36.5 and 41 dB, respectively. The measured front-to-back ratio on the phantom head is significantly larger than that measured in free space because the phantom head is considered a reflector.

C. SAR

The SAR is an important factor in wearable applications; a safe level ensures safe exposure for wearers. An input power of 500 mW is chosen for the SAR simulation. The simulated SARs under US and EU standards at 5.85 and 7 GHz are

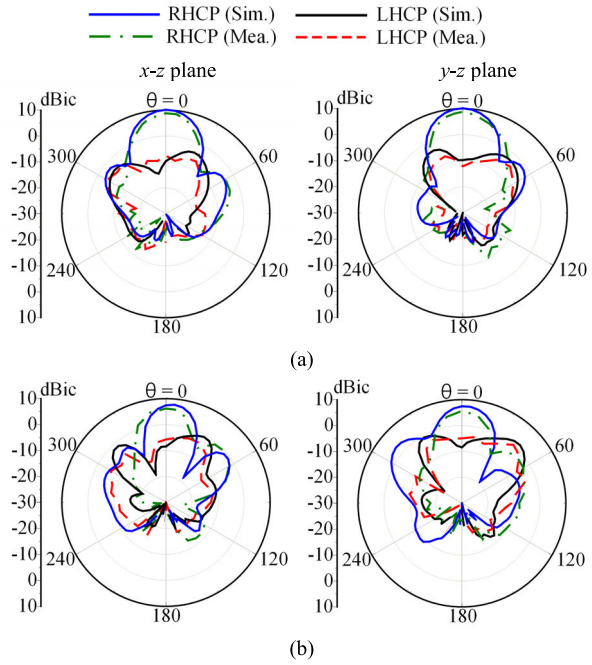

FIGURE 19. Measured radiation pattern at (a) 5.85 GHz and (b) 7.0 GHz in phantom head.

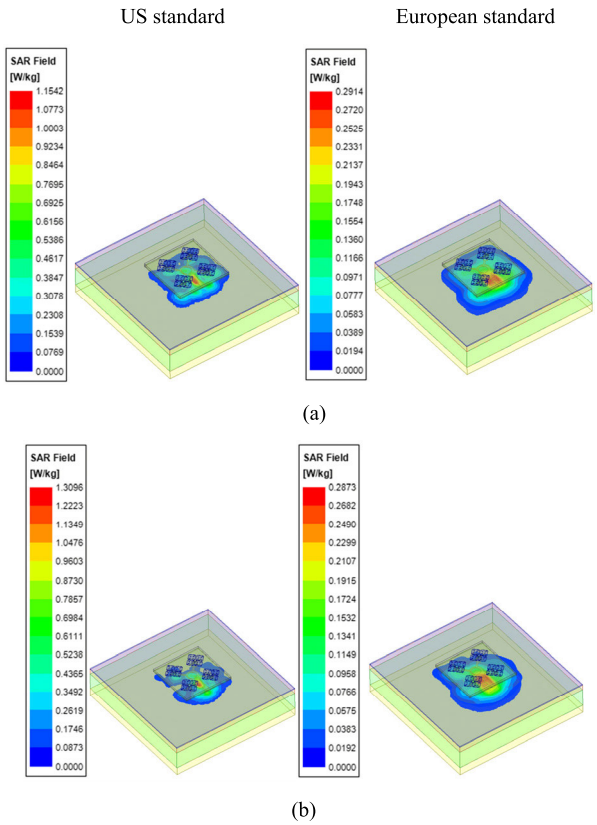

FIGURE 20. Simulated SAR for US and European standards at (a) 5.85 GHz and (b) 7.0 GHz.

shown in Fig. 20. The simulated SARs at 5.85 GHz for US and EU standards are 1.15 W/kg and 0.29 W/kg, respec-

TABLE 2. Comparison with other CP based wearable antennas.

Ref.	Antenna size (λ_0^3)	IBW (%)	ARBW (%)	Gain (dBic)	SAR* (W/kg)	Single/ Array
[2]	0.76 × 0.45 × 0.05	7	1.3	6.1	0.95	Single
[4]	0.4 × 0.4 × 0.12	11.8	6.4	3.5	N/A	Single
[5]	0.46 × 0.46 × 0.17	40.8	22.03	6.5	0.22	Single
[15]*	0.73 × 0.73 × 0.07	43	34	7.5	3.9	Array
Proposal**	0.83 × 0.83 × 0.04	72	47.9	11.2	0.29	Array

* SAR is normalized with an input power of 500 mW for 10g average mass
** λ_0 is the wavelenth at the lowest over the IBW

tively, which are significantly lower than the limit standard of 1.6 W/kg for the US standard and 2 W/kg for the EU standard. Meanwhile, the simulated SARs at 7.0 GHz are 1.3 W/kg and 0.28 W/kg. A comparison of the proposed antenna and other CP wearable antennas is shown in Table 2. The proposed MTS array antenna has a largest among compared antennas but achieved high performances in IBW, ARBW, broadside gain, and low SAR.

V. CONCLUSION

In conclusion, an all-textile broadband circularly polarized MTS array antenna is proposed and demonstrated. Satisfactory broadband performance is achieved by implementing a metasurface radiator and a 90° phase difference sequential series-feeding network. The diagonal slit is etched in the MTS to miniaturize the array antenna. The proposed MTS array antenna is fabricated by a laser cutting technique to produce a highly precise antenna prototype. The antenna performance is verified by measuring it in free space, on the human body, and on a phantom head. The simulation and measurement results are in good agreement.

REFERENCES

[1] U. Ullah, I. B. Mabrouk, and S. Koziel, "A compact circularly polarized antenna with directional pattern for wearable off-body communications," *IEEE Antennas Wireless Propag. Lett.*, vol. 18, pp. 2523–2527, 2019.

[2] H.-R. Zu, B. Wu, Y.-H. Zhang, Y.-T. Zhao, R.-G. Song, and D.-P. He, "Circularly polarized wearable antenna with low profile and low specific absorption rate using highly conductive graphene film," *IEEE Antennas Wireless Propag. Lett.*, vol. 19, pp. 2354–2358, 2020.

[3] H. Xiaomu, S. Yan, and G. A. E. Vandenbosch, "Wearable button antenna for dual-band WLAN applications with combined on and off-body radiation patterns," *IEEE Trans. Antennas Propag.*, vol. 65, no. 3, pp. 1384–1387, Mar. 2017.

[4] T. T. Le, Y.-D. Kim, and T.-Y. Yun, "Wearable pattern-diversity dual-polarized button antenna for versatile on-/off-body communications," *IEEE Access*, vol. 10, pp. 98700–98711, 2022.

[5] T. T. Le, Y.-D. Kim, and T.-Y. Yun, "Bandwidth-enhanced compact circularly-polarized wearable antenna with a magneto-electric dipole," *IEEE Access*, vol. 10, pp. 123225–123232, 2022.

[6] Y. J. Li, Z. Y. Lu, and L. S. Yang, "CPW-fed slot antenna for medical wearable applications," *IEEE Access*, vol. 7, pp. 42107–42112, 2019.

[7] K. W. Lui, O. H. Murphy, and C. Toumazou, "A wearable wideband circularly polarized textile antenna for effective power transmission on a wirelessly-powered sensor platform," *IEEE Trans. Antennas Propag.*, vol. 61, no. 7, pp. 3873–3876, Jul. 2013.

[8] Z. H. Jiang, D. E. Brocker, P. E. Sieber, and D. H. Werner, "A compact, low-profile metasurface-enabled antenna for wearable medical body-area network devices," *IEEE Trans. Antennas Propag.*, vol. 62, no. 8, pp. 4021–4030, Aug. 2014.

[9] G.-P. Gao, C. Yang, B. Hu, R.-F. Zhang, and S.-F. Wang, "A wearable PIFA with an all-textile metasurface for 5 GHz WBAN applications," *IEEE Antennas Wireless Propag. Lett.*, vol. 18, pp. 288–292, 2019.

[10] Y. Wang and A. Zhang, "Dual circularly polarized Fabry–Pérot resonator antenna employing a polarization conversion metasurface," *IEEE Access*, vol. 9, pp. 44881–44887, 2021.

[11] T. T. Le, Y.-D. Kim, and T.-Y. Yun, "All-textile enhanced-bandwidth polarization-conversion antenna using a nonuniform metasurface," *IEEE Antennas Wireless Propag. Lett.*, vol. 22, pp. 2432–2436, 2023.

[12] S.-K. Lin and Y.-C. Lin, "A compact sequential-phase feed using uniform transmission lines for circularly polarized sequential-rotation arrays," *IEEE Trans. Antennas Propag.*, vol. 59, no. 7, pp. 2721–2724, Jul. 2011.

[13] Y. Li, Z. Zhang, and Z. Feng, "A sequential-phase feed using a circularly polarized shorted loop structure," *IEEE Trans. Antennas Propag.*, vol. 61, no. 3, pp. 1443–1447, Mar. 2013.

[14] M. Wang, W. Wu, and Z. Shen, "Bandwidth enhancement of antenna arrays utilizing mutual coupling between antenna elements," *Int. J. Antennas Propag.*, vol. 2010, pp. 1–9, Jun. 2010.

[15] Y. Chen, X. Liu, Y. Fan, and H. Yang, "Wearable wideband circularly polarized array antenna for off-body applications," *IEEE Antennas Wireless Propag. Lett.*, vol. 21, pp. 1051–1055, 2022.

[16] F. H. Lin and Z. N. Chen, "Low-profile wideband metasurface antennas using characteristic mode analysis," *IEEE Trans. Antennas Propag.*, vol. 65, no. 4, pp. 1706–1713, Apr. 2017.

[17] G. Gao, R.-F. Zhang, W.-F. Geng, H.-J. Meng, and B. Hu, "Characteristic mode analysis of a nonuniform metasurface antenna for wearable applications," *IEEE Antennas Wireless Propag. Lett.*, vol. 19, pp. 1355–1359, 2020.

[18] Y. Shi and W. J. Wang, "A transparent wideband dual-polarized antenna for sub-6 GHz application," *IEEE Antennas Wireless Propag. Lett.*, vol. 21, pp. 2020–2024, 2022.

[19] T. T. Le and T.-Y. Yun, "Miniaturization of a dual-band wearable antenna for WBAN applications," *IEEE Antennas Wireless Propag. Lett.*, vol. 19, pp. 1452–1456, 2020.

[20] S. Liu, D. Yang, and J. Pan, "A low-profile broadband dual-circularly-polarized metasurface antenna," *IEEE Antennas Wireless Propag. Lett.*, vol. 18, pp. 1395–1399, 2019.

[21] X. Gao, G. Tian, Z. Shou, and S. Li, "A low-profile broadband circularly polarized patch antenna based on characteristic mode analysis," *IEEE Antennas Wireless Propag. Lett.*, vol. 20, pp. 214–218, 2021.

[22] J.-C. Liu, B.-H. Zeng, L. Badjie, S. Drammeh, S.-S. Bor, T.-F. Hung, and D.-C. Chang, "Single-feed circularly polarized aperture-coupled stack antenna with dual-mode square loop radiator," *IEEE Antennas Wireless Propag. Lett.*, vol. 9, pp. 887–890, 2010.

[23] P. Sharma and K. Gupta, "Analysis and optimized design of single feed circularly polarized microstrip antennas," *IEEE Trans. Antennas Propag.*, vol. AP-31, no. 6, pp. 949–955, Nov. 1983.

[24] Y.-M. Zhang and J.-L. Li, "Analyses and full-duplex applications of circularly polarized OAM arrays using sequentially rotated configuration," *IEEE Trans. Antennas Propag.*, vol. 66, no. 12, pp. 7010–7020, Dec. 2018.

[25] *Calculation of the Dielectric Properties of Body Tissues in the Frequency Range 10 Hz-100 GHz*. Italian National Research Council, Institute for Applied Physics. Accessed: Jul. 13, 2023. [Online]. Available: http://niremf.ifac.cnr.it/docs/DIELECTRIC/Report.html

TU TUAN LE received the B.S. degree in electronics and telecommunications from the Hanoi University of Science and Technology, Hanoi, Vietnam, in 2013, and the Ph.D. degree from the Department of Electronics and Electrical Engineering, Dongguk University, Seoul, South Korea. He is currently with Hanyang University, Seoul, as a Research Assistant Professor. His current research interests include RF energy harvesting, wearable antenna, circularly polarized antennas, reconfigurable antennas, and multiband/broadband planar antennas for various wireless applications.

YONG-DEOK KIM received the B.S. degree in information and communication engineering from Hoseo University, South Korea, in 2020. He is currently pursuing the Ph.D. degree with the Department of Electronics Engineering, Hanyang University, Seoul, South Korea. His current research interests include circularly polarized antennas, wearable antennas, multiband antennas, and on-chip antennas for various wireless applications.

TAE-YEOUL YUN (Member, IEEE) received the Ph.D. degree from the Department of Electrical Engineering, Texas A&M University, College Station, TX, USA, in 2001. From 1989 to 1996, he was with the Optical Telecommunication System Group, ETRI, Daejon, South Korea, where he developed 2.5- and 10-Gb/s systems. From 2001 to 2003, he was an MMIC Designer with Triquint Semiconductor, Dallas, TX, USA. Since 2003, he has been a Professor with Hanyang University, Seoul, South Korea. His research interests include RFICs, antennas, and wireless/optical high-speed communication systems.